This manuscript was accepted by Phys. Fluids. Click here to see the version of record.

Flow-induced resonant shear-wave instability between a viscoelastic fluid and an elastic solid

Parag Joshi[1] and V. Shankar[1, a)]
Department of Chemical Engineering, Indian Institute of Technology, Kanpur 208016, India

Linear stability analysis of plane Couette flow of a viscoelastic, upper-convected Maxwell (UCM) fluid past a deformable elastic solid is carried out in the low Reynolds number limit using both numerical and asymptotic techniques. The UCM fluid is characterized by its viscosity η, density ρ, and relaxation time τ_R, whereas the deformable solid is considered to be a linear elastic solid of shear modulus G. The asymptotic analysis is performed in the $Re \ll 1$ limit where $Re = \rho V R/\mu$ is the Reynolds number, V is the top plate velocity, and R is the thickness of the fluid. Both asymptotic and numerical approaches are used to understand the effect of solid elasticity, represented by the dimensionless parameter Γ, and fluid elasticity, characterized by the Weissenberg number W, on the growth rate of a class of modes with high frequencies (compared to the imposed shear rate, termed high-frequency Gorodtsov-Leonov, or 'HFGL' modes) in the $Re \ll 1$ limit. Here, the dimensionless groups are defined as $W = \tau_R V/R$ and $\Gamma = \eta V/GR$. The results obtained from the numerical analysis show that there is an interaction between the shear waves in the fluid and the elastic solid, which are coupled via the continuity conditions at the interface. The interaction is particularly pronounced when $W = \Gamma$, strongly reminiscent of resonance. The resonance-induced interaction leads to shear waves in the coupled system with a decay rate of $c_i = -1/[2k(W + \Gamma)]$. In this case, it is not possible to differentiate the fluid and solid shear waves individually and the coupled fluid-solid system behaves as a single composite material. The leading order asymptotic analysis suggests that the growth rate of the HFGL modes is proportional to W^2, for $W \ll 1$. The asymptotic analysis, up to first correction, shows an oscillating behaviour of c_i with increase in Γ, in agreement with the results from our numerical approach. In addition, we also carry out an asymptotic analysis in the no-flow, but nonzero inertia limit to illustrate the role played by the imposed flow on the instability of the shear waves. It is found that, at leading order, the wavespeed for the coupled fluid-solid problem is neutrally stable in the absence of flow. Thus, the unstable resonant modes in the coupled fluid-solid system are shown to be driven by the imposed flow.

[a)]Author for correspondence; E-mail: vshankar@iitk.ac.in

I. INTRODUCTION

There are many instances in which fluid flows occur past soft, deformable solid surfaces, such as in biological systems including blood flow in the circulatory[1] and respiratory system[2], and more recently in flow through microfluidic devices fabricated using soft, elastomeric platforms[3]. Recent experimental work[4–6] has shown that deformable solid surfaces can be used to trigger hydrodynamic instabilities which can be exploited to enhance micromixing. In the past two decades, several studies, both theoretical and experimental[4,7–13] have been carried out to understand the effect of deformable walls on the stability of the flow. Experimental studies have demonstrated the existence of instabilities in Newtonian flows through deformable channels and tubes[9,14–16], in qualitative agreement with theoretical predictions. These studies have shown that the presence of the deformable surface renders the flow unstable at Reynolds numbers where flow through rigid surfaces is in the laminar regime. There are qualitatively different instabilities in different parametric regimes[17], depending on the extent of wall deformability.

Interestingly, even in the limit of very low Reynolds numbers, it is possible to have instabilities in flow past deformable solid surfaces[10,18,19]. Kumaran et. al.[10] carried out the first theoretical study to demonstrate an instability, even in the creeping-flow limit, for plane Couette flow of a Newtonian fluid past a linear elastic solid. They predicted an instability in the absence of fluid and solid inertia and normal stress discontinuities. Disturbances at the interface were shown to derive energy from the mean flow as a result of the work done by the mean flow at the interface and inertia is not essential to produce an instability. It has also been reported that the minimum shear rate to destabilize the surface fluctuations depends on nondimensional solid thickness H, ratio of gel to the fluid viscosity $\frac{\eta_g}{\eta_r}$ and $\frac{\gamma}{\Gamma R}$, where γ is the surface tension, Γ is the solid elasticity parameter and R is fluid thickness.

While the earlier study[10] used the linear elastic model for the wall deformation, Gkains and Kumar[11] used the neo-Hookean model to analyze the stability of plane Couette flow of a Newtonian fluid past a deformable solid in the creeping-flow limit. They pointed out that in parametric regimes where the flow is unstable[10], the base state deformation gradients in the elastic solid are large and hence the use of a linear elastic model is not self-consistent. Using a frame-invariant (non-linear) neo-Hookean model, they showed that the instability predicted in the creeping-flow limit using the linear elastic model is still present, but the nonlinear rheological properties of the solid play an important role in triggering a new short-wave instability. The first normal difference in the base state of a neo-Hookean solid, which was absent in linear elastic model, causes an instability different in behaviour from that observed in the flow past a linear elastic solid[10]. In particular, they showed that, when the interfacial tension is zero, the first normal stress difference gives rise to a short-wave instability. They further examined the effect of nondimensional parameters such as solid thickness, strain rate and interfacial tension on the instability.

Gorodtsov and Leonov[20] carried out arguably the first linear stability analysis of a UCM fluid undergoing plane Couette flow in a rigid channel. In the creeping-flow limit, they showed that there are two stable, discrete modes at nonzero W. These discrete modes are referred henceforth as zero Reynolds number Gorodtsov-Leonov (ZRGL) modes, signifying their presence even in the absence of fluid inertia. For small but nonzero $Re \ll 1$, they carried out an asymptotic analysis using $\epsilon = (Re/W)^{1/2}$ as the small parameter and analytically solved the system of linearized governing equations. They reported an instability at high wavenumbers which was later shown[21] to be incorrect. Their asymptotic analysis also showed that, in the $Re \ll 1$ limit, the UCM fluid has numerous stable discrete eigenmodes with a wide range of wavespeed c_r while having a similar decay rate of $c_i = -1/(2kW)$. We refer to these modes as 'high-freuquency Gorodtsov-Leonov'

(HFGL) modes. Physically these modes correspond to damped shear waves in a viscoelastic fluid, and the wavespeed of the HFGL modes correspond to the dimensional shear wave speed $\sqrt{G/\rho}$, where $G = \eta/\lambda$ is the shear modulus of the viscoelastic fluid. The numerical study of[21] conclusively showed that plane Couette flow of a UCM fluid is always stable in the Re–W parameter space.

Shankar and Kumar[18] performed a linear stability analysis for UCM plane Couette flow past a linear elastic solid in creeping-flow limit. They found that only one of the two ZRGL modes becomes unstable due to wall deformability at a significantly high H and W for small wavenumbers. They argued that, for $W \to 0$, and at sufficiently higher value of Γ, the unstable ZRGL mode smoothly continues into the Newtonian instability found for flow past a linear elastic solid first predicted by Kumaran et. al.[10]. Similarly, in the rigid-wall limit ($\Gamma \to 0$), the unstable mode becomes the stable ZRGL mode, which shows that lowering the Γ stabilizes the system. Kumar and Shankar[22] performed stability analysis for UCM plane Couette flow past a deformable wall using both asymptotic and numerical approaches to analyze the role of wall elasticity on the HFGL modes of Gorodtsov and Leonov[20]. They predicted an instability in the $W \sim O(1)$ limit and for $\epsilon = Re^{1/2}$. They showed that it is possible to obtain an unstable eigenvalue even at very low Γ, corresponding to very low wall deformability. However, their analysis was restricted to the calculation of the leading order contribution to the asymptotic expansion of the dynamical quantities and the complex wavespeed. In the present work, the first correction to the wave speed is analytically obtained which significantly improves the theoretically predictions on the stability of the system. Kumar and Shankar[22] also examined the stability of UCM plane Couette flow past a linear elastic solid in the finite Reynolds number regime using numerical techniques. They reported an instability for $Re \ll 1$ and $W \sim O(1)$ at low value of Γ. However, they used only a shooting method in their asymptotic analysis for low-Re limit, which cannot capture all the unstable modes present in the system. Chokshi and Kumaran[23] performed linear and weakly nonlinear stability analyses for Couette flow of viscoelastic fluid past a neo-Hookean solid in the creeping-flow limit where they analyzed the effect of fluid elasticity on critical imposed shear rate Γ_c and found that the critical Γ increase with an increase in W, where W is the Weissenberg number. The flow is stable for dilute polymer solutions ($\beta > 0.5$), where β is the ratio of solvent viscosity to the total viscosity of the polymer solution, beyond W_{max} and W_{max} is proportional to H. However, for concentrated polymer solutions, the system is unstable at any W for Γ larger than Γ_c. There have been some recent work[24–28] that analyzed the role of shear thinning on instabilities in flow past a deformable solid, but used inelastic constitutive relations such as the power-law or Carreau models which neglect the elastic nature of the polymeric liquid. The focus in this study is exclusively on the role of elasticity in the fluid on the instabilities on flow past a deformable solid, and hence we ignore shear thinning effects here. The phenomenon identified in this study is absent for inelastic fluids.

In this work, we have overcome the limitations of the earlier work[22] on both asymptotic and numerical fronts: (i) From the standpoint of asymptotic analysis, we have gone beyond the earlier work by extending the analysis to calculate the first correction to the wavespeed, leading to more insight into the origin of the unstable modes, (ii) In the numerical front, we have now used a spectral numerical method (in addition to the shooting procedure of Ref. 22), which gives a comprehensive picture of all the unstable (and stable) modes in the spectrum. The spectral analysis in this paper demonstrates how the shear waves of the fluid and the solid interact with each other. The respective fluid and solid shear wave speeds are proportional to $\sqrt{\frac{\eta}{\tau_R \rho}}$ and $\sqrt{\frac{G}{\rho}}$ respectively, where τ_R is the fluid relaxation time, ρ is the density of the fluid, η viscosity of the fluid, and G is the shear modulus of the deformable surface, whereas the first correction to the wave speed

predicts the instability of the system.

The rest of the paper is structured as follows: Section II contains the underlying governing equations and asymptotic analysis in both flow and no-flow conditions. Results obtained by the numerical and asymptotic analysis are discussed in Sec. III, and the major conclusions of the present study are summarized in Sec. IV.

II. PROBLEM FORMULATION

We consider the plane Couette flow of a viscoelastic fluid of thickness R past a deformable surface of width HR, where H is the ratio of the solid to the fluid thickness. The fluid is modelled using the UCM model whereas the deformable solid is considered to be a linear elastic solid. We use R to non-dimensionalize lengths. The deformable solid is affixed on a rigid stationary plate at $z = -H$, where z ranges from 1 to $-H$, is the scaled domain of the coupled flow system. The fluid is bounded between the deformable solid at $z = 0$ and a rigid top plate at $z = 1$. The rigid top plate moves in the x-direction as shown in the Figure 1. The material constants of the viscoelastic fluid are viscosity η_f and the relaxation time τ_R whereas the solid is characterized by viscosity, η_g, and shear modulus, G. Both the fluid and the solid are coupled through the interface at $z = 0$.

Equations that govern the flow are nondimensionalized using the following scales: R for lengths and displacements, V for velocities, R/V for time, and $\eta V/R$ for pressure and stresses. The resulting nondimensional mass and momentum balance equations for fluid take the following

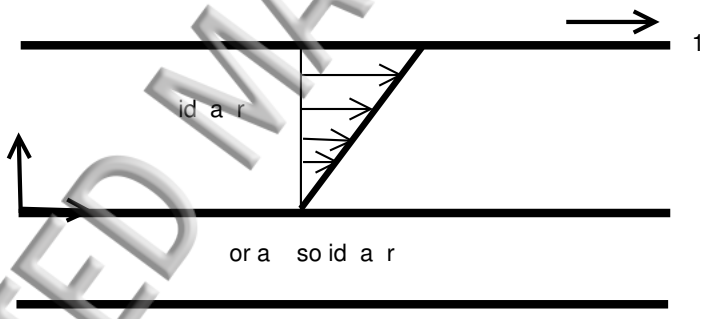

FIG. 1: Schematic diagram showing nondimensional coordinate system for Couette flow of a UCM fluid past a deformable solid

form:

$$\partial_i v_i = 0, \tag{1}$$

$$Re\left[\partial_t + v_j\partial_j\right] v_i = -\partial_i p_f + \partial_j \tau_{ij}, \tag{2}$$

where, $\partial_t \equiv \partial/\partial t$, v_i is the velocity field, Re is the Reynolds number $\rho V R/\eta$, $p_f\delta_{ij}$ is the isotropic pressure field in the fluid, and τ_{ij} is the extra stress tensor. The indices i, j can take the values x, z for direction. The extra stress tensor for the UCM model is given by the following consitutive relation:

$$W[\partial_t\tau_{ij} + v_k\partial_k\tau_{ij} - \partial_k v_i\tau_{kj} - \partial_k v_j\tau_{ki}] + \tau_{ij} = (\partial_i v_j + \partial_j v_i), \tag{3}$$

where, $W = \tau_R V/R$ is the Weissenberg number which is defined as the ratio of elastic forces to the viscous forces.

The deformable solid is assumed to be incompressible and nonporous, which is modelled using the linear viscoelastic constitutive relation. While Gkanis and Kumar[11] have shown the importance of using a non-linear solid, we use the linear elastic model to bring out the physical mechanism of the resonant instability discussed below. Further, the instability is predicted to occur at small values of base-state deformation gradients, and the linear elastic model is expected to be a self-consistent approximation in this problem. In this limit, both linear elastic model and neo-Hookean model predict qualitatively similar results[11]. Furthermore, the density ratio of the fluid to the solid is taken to be unity. The nondimensionalized incompressibility condition and the momentum conservation equation for the flexible surface are given by

$$\partial_i u_i = 0, \tag{4}$$

$$Re\left(\partial_t^2 u_i\right) = -\partial_j \Pi_{ij}, \tag{5}$$

where u_i is the displacement field in the solid and Π_{ij} is the total stress tensor which is a sum of isotropic pressure, $-p_g\delta_{ij}$, and deviatoric stress tensor, σ_{ij}. The total stress tensor and deviatoric stress tensors are given by

$$\Pi_{ij} = -p_g\delta_{ij} + \sigma_{ij}, \tag{6}$$

$$\sigma_{ij} = \left[\frac{1}{\Gamma} + \eta_r\partial_t\right](\partial_i u_j + \partial_j u_i). \tag{7}$$

Here, $\Gamma = V\eta/(GR)$ is the nondimensional elasticity parameter for the solid, and the limit of $\Gamma \to 0$ represents a rigid solid.

A. Base state

The unidirectional, fully developed, steady base state velocity and stress field profiles for the fluid are given (in dimensionless form) by

$$\bar{v}_x = z \qquad \bar{v}_z = 0, \tag{8}$$

$$\bar{\tau}_{xx} = 2W \qquad \bar{\tau}_{zz} = 0 \qquad \bar{\tau}_{xz} = \bar{\tau}_{zx} = 1. \tag{9}$$

Similarly, the base state displacement and stress field profiles for the deformable solid are

$$\bar{u}_x = \Gamma(z + H) \qquad \bar{u}_z = 0, \tag{10}$$

$$\bar{\sigma}_{xx} = \bar{\sigma}_{zz} = 0, \qquad \bar{\sigma}_{xz} = \bar{\sigma}_{zx} = 1. \tag{11}$$

B. Linear Stability Analysis

A temporal linear stability analysis is performed to examine the stability of a UCM plane Couette flow past a deformable wall. The dynamical quantities of aforementioned governing equations, Eqs. 1-7, and the set of boundary conditions, Eqs. 8-11, are perturbed about the base state. The dynamical quantities, after the imposition of perturbations, are represented as $f = \overline{f} + f'$, where f

represents any of $v_z, v_x, p_f, \tau_{xx}, \tau_{xz}, \tau_{zz}, u_z, u_x$, or p_g. The overbar denotes base state and prime ($'$) denotes perturbed state quantity. The perturbed form of all the dynamical quantities are substituted in the governing equations and these are then linearlized. Furthermore, perturbed quantities are represented in the form of Fourier modes

$$f(x,z,t) = \tilde{f}(z)e^{[ik(x-ct)]}, \tag{12}$$

where k is the wavenumber, and $c = c_r + ic_i$ is the complex wavespeed of perturbations. If $c_i > 0$ (< 0) the flow is temporally unstable (stable). After linearization and normal mode decomposition, the equations governing the dynamics of perturbations of the fluid take the following form

$$d_z\tilde{v}_z + ik\tilde{v}_x = 0, \tag{13a}$$
$$-ik\tilde{p}_f + ik\tilde{\tau}_{xx} + d_z\tilde{\tau}_{xz} = Re[ik(z-c)\tilde{v}_x + \tilde{v}_z], \tag{13b}$$
$$-d_z\tilde{p}_f + d_z\tilde{\tau}_{xx} + ik\tilde{\tau}_{xz} = Re[ik(z-c)\tilde{\mathbf{v}}_\mathbf{z}], \tag{13c}$$
$$\tilde{\tau}_{zz}[1 + ikW(z-c)] = 2d_z\tilde{v}_z + 2ikW\tilde{v}_z, \tag{13d}$$
$$\tilde{\tau}_{xz}[1 + ikW(z-c)] = (d_z\tilde{v}_x + ik\tilde{v}_z) + W(\tilde{\tau}_{zz} + 2ikW\tilde{v}_z), \tag{13e}$$
$$\tilde{\tau}_{xx}[1 + ikW(z-c)] = 2ik\tilde{v}_x + W(2\tilde{\tau}_{xz} + 4ikW\tilde{v}_x + 2d_z\tilde{v}_x). \tag{13f}$$

The linearized governing equations for the deformable solid are given by

$$d_z\tilde{u}_z + ik\tilde{u}_x = 0, \tag{14a}$$
$$-ik\tilde{p}_g + \left(\frac{1}{\Gamma} - ikc\eta_r\right)(d_z{}^2 - k^2)\tilde{u}_x = -Rek^2c^2\tilde{u}_x, \tag{14b}$$
$$-d_z\tilde{p}_g + \left(\frac{1}{\Gamma} - ikc\eta_r\right)(d_z{}^2 - k^2)\tilde{u}_z = -Rek^2c^2\tilde{u}_z. \tag{14c}$$

The linearized governing equations are solved in conjunction with the boundary conditions mentioned below. The no-slip and no-penetration conditions at $z = 1$ and $z = -H$, are

$$\tilde{v}_z = \tilde{v}_x = 0 \qquad at \;\; z = 1, \tag{15}$$
$$\tilde{u}_z = \tilde{u}_x = 0 \qquad at \;\; z = -H. \tag{16}$$

The continuity conditions for velocity and stresses at the interface are Taylor expanded about the base-state location of the interface at $z = 0$ to yield

$$\tilde{v}_z = \frac{\partial\tilde{u}_z}{\partial t}, \tag{17}$$
$$\tilde{v}_x + \tilde{u}_z\frac{d\bar{v}_x}{dz} = \frac{\partial\tilde{u}_x}{\partial t}, \tag{18}$$
$$-\tilde{p}_f + \tilde{\tau}_{zz} = -\tilde{p}_g + 2\left[\frac{1}{\Gamma} + \eta_r\frac{\partial}{\partial t}\right]\frac{\partial\tilde{u}_z}{\partial z}, \tag{19}$$
$$\tilde{\tau}_{xz} - 2W\frac{\partial\tilde{u}_z}{\partial x} = \left[\frac{1}{\Gamma} + \eta_r\frac{\partial}{\partial t}\right]\left[\frac{\partial\tilde{u}_x}{\partial z} + \frac{\partial\tilde{u}_z}{\partial x}\right]. \tag{20}$$

The differential eigenvalue problem arising out of the linearized governing equations, Eqs. 13a-14c along with boundary conditions, Eqs. 15-20, is solved numerically using a Chebyshev spectral collocation method. This results in a generalized eigenvalue problem of the form

$$c^2\,[C]\,a + \;c\,[B]\,a + [A]\,a \;= 0, \tag{21}$$

where, A, B and C are matrices of dimension $9N \times 9N$, with N being the number of collocation points. The eigenvalue problem is solved using the built-in function *polyeig* of MATLAB.

C. Asymptotic analysis

Kumar and Shankar[22] carried out an asymptotic analysis to examine the stability of UCM plane Couette flow past a linear elastic solid . They considered the $Re \ll 1$ limit with $W \sim O(1)$ and wavespeed $c \sim Re^{-1/2} \gg 1$ and reported that it is possible to render all HFGL modes unstable due to wall deformability. Now, for the same $Re \ll 1$ limit, we consider that W can take any value provided that $(Re/W)^{1/2}$ is $\ll 1$, the small parameter ϵ scales as $Re^{1/2}$. With the aforementioned limits and assumptions, the complex wavespeed can be asymptotically expanded as

$$c = Re^{-1/2}c^{(0)} + c^{(1)} + ... \tag{22}$$

Similarly, perturbation velocities can be asymptotically expanded as

$$\tilde{v}_z = Re^{-1/2}\tilde{v}_z^{(0)} + \tilde{v}_z^{(1)} + ... \tag{23}$$
$$\tilde{v}_x = Re^{-1/2}\tilde{v}_x^{(0)} + \tilde{v}_x^{(1)} + ... \tag{24}$$

The pressure field in the fluid is given by x-momentum equation whereas the stress components are given by constitutive relation. Similar to the perturbation velocities, asymptotic series expansion of the pressure and stress components for the fluid are given by

$$\tilde{\tau}_{xx} = \tilde{\tau}_{xx}^{(0)} + Re^{1/2}\tilde{\tau}_{xx}^{(1)} + ... \tag{25}$$
$$\tilde{\tau}_{xz} = \tilde{\tau}_{xz}^{(0)} + Re^{1/2}\tilde{\tau}_{xz}^{(1)} + ... \tag{26}$$
$$\tilde{\tau}_{zz} = \tilde{\tau}_{zz}^{(0)} + Re^{1/2}\tilde{\tau}_{zz}^{(1)} + ... \tag{27}$$
$$\tilde{p}_f = \tilde{p}_f^{(0)} + Re^{1/2}\tilde{p}_f^{(1)} + ... \tag{28}$$

Upon substituting above expansions for velocity, pressure and stress quantities in the linearized governing equations (Eqs. 13a-13f), we obtain the following equations at leading order

$$-ikWc^{(0)}\tilde{\tau}_{zz}^{(0)} = 2d_z\tilde{v}_z^{(0)} + 2ikW\tilde{v}_z^{(0)}, \tag{29}$$
$$-ikWc^{(0)}\tilde{\tau}_{xz}^{(0)} = d_z\tilde{v}_x^{(0)} + ik\tilde{v}_z^{(0)} + 2ikW^2\tilde{v}_z^{(0)}, \tag{30}$$
$$-ikWc^{(0)}\tilde{\tau}_{xx}^{(0)} = 2ik\tilde{v}_x^{(0)} + 2Wd_z\tilde{v}_x^{(0)} + 4ikW^2\tilde{v}_x^{(0)}, \tag{31}$$
$$-ik\tilde{p}_f^{(0)} = -ik\tilde{\tau}_{xx}^{(0)} - ikc^{(0)}\tilde{v}_x^{(0)} - d_z\tilde{\tau}_{xz}^{(0)}, \tag{32}$$
$$-d_z\tilde{p}_f^{(0)} = -d_z\tilde{\tau}_{zz}^{(0)} - ikc^{(0)}\tilde{v}_z^{(0)} - ik\tilde{\tau}_{xz}^{(0)}, \tag{33}$$
$$d_z\tilde{v}_z^{(0)} + ik\tilde{v}_x^{(0)} = 0. \tag{34}$$

A final fourth order ODE in perturbation velocity $\tilde{v}_z^{(0)}$ obtained by merging Eqs. 29-34 is given by

$$[d_z^2 - k^2][d_z^2 + 2ikWd_z + k^2(c^{(0)})^2W - k^2 - 2k^2W^2]\tilde{v}_z^{(0)} = 0. \tag{35}$$

The above ODE is analytically solved to obtain the perturbation velocity field $\tilde{v}_z^{(0)}$

$$\tilde{v}_z^{(0)} = A_1\exp^{[kz]} + A_2\exp^{[-kz]} + A_3\exp^{[-ikW+k\sqrt{1-(c^{(0)})^2W+W^2}]z} + A_4\exp^{[-ikW-k\sqrt{1-(c^{(0)})^2W+W^2}]z}. \tag{36}$$

The perturbed dynamical quantities of the deformable solid are asymptotically expanded in a similar manner to that of the fluid. The asymptotic series expansion of the displacement and pressure fields are given by

$$\tilde{u}_z = \tilde{u}_z^{(0)} + Re^{1/2}\tilde{u}_z^{(1)} + ... \tag{37}$$
$$\tilde{u}_x = \tilde{u}_x^{(0)} + Re^{1/2}\tilde{u}_x^{(1)} + ... \tag{38}$$
$$\tilde{p}_g = \tilde{p}_g^{(0)} + Re^{1/2}\tilde{p}_g^{(1)} + ... \tag{39}$$

Upon substituting the above expansions in the linearized governing equations eqs.$14a$-$14c$, we obtain the following equations at leading order

$$d_z\tilde{u}_z^{(0)} + ik\tilde{u}_x^{(0)} = 0, \tag{40}$$
$$-ik\tilde{p}_g^{(0)} + \frac{1}{\Gamma}(d_z^2 - k^2)\tilde{u}_x^{(0)} = -k^2(c^{(0)})^2\tilde{u}_x^{(0)}, \tag{41}$$
$$-d_z\tilde{p}_g^{(0)} + \frac{1}{\Gamma}(d_z^2 - k^2)\tilde{u}_z^{(0)} = -k^2(c^{(0)})^2\tilde{u}_z^{(0)}. \tag{42}$$

Upon merging the above derived leading order linearized governing equations, we obtain a 4^{th}-order ODE

$$[d_z^2 - k^2][d_z^2 - k^2 + k^2\Gamma(c^{(0)})^2]\tilde{u}_z^{(0)} = 0, \tag{43}$$

which is analytically solved to get the displacement field $\tilde{u}_z^{(0)}$:

$$\tilde{u}_z^{(0)} = B_1\exp^{[kz]} + B_2\exp^{[-kz]} + B_3\exp^{[-ikW + k\sqrt{1-(c^{(0)})^2\Gamma}]z} + B_4\exp^{[-ikW - k\sqrt{1-(c^{(0)})^2\Gamma}]z}. \tag{44}$$

The linearized equations at leading order for both the fluid and the solid are then numerically solved to obtain wavespeed using the following sets of boundary and interface conditions.

$$\tilde{v}_z^{(0)} = \tilde{v}_x^{(0)} = 0 \quad at \quad z = 1, \tag{45}$$
$$\tilde{u}_z^{(0)} = \tilde{u}_x^{(0)} = 0 \quad at \quad z = -H, \tag{46}$$

Interface conditions:

$$\tilde{v}_z^{(0)} = -ikc^{(0)}\tilde{u}_z^{(0)}, \tag{47}$$
$$\tilde{v}_x^{(0)} = -ikc^{(0)}\tilde{u}_x^{(0)}, \tag{48}$$
$$\tilde{\tau}_{xz}^{(0)} - 2ikW\tilde{u}_z^{(0)} = \frac{1}{\Gamma}(d_z\tilde{u}_x^{(0)} + ik\tilde{u}_z^{(0)}), \tag{49}$$
$$-\tilde{p}_f^{(0)} + \tilde{\tau}_{zz}^{(0)} = -\tilde{p}_g^{(0)} + \frac{2}{\Gamma}d_z\tilde{u}_z^{(0)}. \tag{50}$$

In Sec. 4 of their work, Kumar and Shankar[22] showed that for $\Gamma \ll 1$, the c_i data obtained by leading order asymptotic analysis do not match with the numerical results. This discrepancy suggests that the leading order asymptotic analysis alone can not predict stability of the coupled flow system. This lacuna is addressed in the present work by obtaining the first correction to the wavespeed

by solving the governing equations derived in first correction terms. After using similar asymptotic series expansions (Eqs. 22-28) for perturbation quantities in the fluid, we obtain the following equations at first correction

$$[1+ikW(z-c^{(1)})]\tilde{\tau}_{zz}^{(0)} - ikWc^{(0)}\tilde{\tau}_{zz}^{(1)} = 2d_z\tilde{v}_z^{(1)} + 2ikW\tilde{v}_z^{(1)}, \tag{51}$$

$$[1+ikW(z-c^{(1)})]\tilde{\tau}_{xz}^{(0)} - ikWc^{(0)}\tilde{\tau}_{xz}^{(1)} = d_z\tilde{v}_x^{(1)} + ik\tilde{v}_z^{(1)} + 2ikW^2\tilde{v}_z^{(1)} + W\tilde{\tau}_{zz}^{(0)}, \tag{52}$$

$$[1+ikW(z-c^{(1)})]\tilde{\tau}_{xx}^{(0)} - ikWc^{(0)}\tilde{\tau}_{xx}^{(1)} = 2ik\tilde{v}_x^{(1)} + 4ikW^2\tilde{v}_x^{(1)} + 2Wd_z\tilde{v}_x^{(1)} + 2W\tilde{\tau}_{xz}^{(0)}, \tag{53}$$

$$ikz\tilde{v}_x^{(0)} - ikc^{(0)}\tilde{v}_x^{(1)} - ikc^{(1)}\tilde{v}_x^{(0)} + \tilde{v}_z^{(0)} = -ik\tilde{p}_f^{(1)} + ik\tilde{\tau}_{xx}^{(1)} + d_z\tilde{\tau}_{xz}^{(1)}, \tag{54}$$

$$-d_z\tilde{p}_f^{(1)} + d_z\tilde{\tau}_{zz}^{(1)} + ik\tilde{\tau}_{xz}^{(1)} = ikz\tilde{v}_z^{(0)} - ikc^{(0)}\tilde{v}_z^{(1)} - ikc^{(1)}\tilde{v}_z^{(0)}. \tag{55}$$

Upon simplifying Eqs. 51-55, we obtain the following 4^{th}-order nonhomogeneous ODE

$$[d_z^2-k^2][d_z^2+2ikWd_z+k^2(c^{(0)})^2W-k^2-2k^2W^2]\tilde{v}_z^{(1)} = e(z)C_3 + f(z)C_4 + g(z)C_1 + l(z)C_2 \tag{56}$$

where,

$$e(z) = \frac{4k^3W(W-i)\exp^{[-kz]}}{c^{(0)}} \tag{57}$$

$$f(z) = \frac{4k^3W(W-i)\exp^{[kz]}}{c^{(0)}} \tag{58}$$

$$g(z) = [ik^3W(c^{(0)})^3 - 2ik^3W^2c^{(0)} + 2k^4W^2(c^{(0)})^3(c^{(1)}-z) - 4ic^{(0)}k^4W^2(c^{(1)}-z)\sqrt{1-(c^{(0)})^2W+W^2})] \exp^{[-ikW-k\sqrt{1-(c^{(0)})^2W+W^2}]z} \tag{59}$$

$$l(z) = [ik^3W(c^{(0)})^3 - 2ik^3W^2c^{(0)} + 2k^4W^2(c^{(0)})^3(c^{(1)}-z) + 4ic^{(0)}k^4W^2(c^{(1)}-z)\sqrt{1-(c^{(0)})^2W+W^2})] \exp^{[-ikW+k\sqrt{1-(c^{(0)})^2W+W^2}]z}. \tag{60}$$

If we compare Eq. 35 and 56, it turns out that the differential operator which is operating on $\tilde{v}_z^{(0)}$ is similar to the one operating on $\tilde{v}_z^{(1)}$. The solution of the nonhomogeneous ODE eq.56, gives a

This manuscript was accepted by Phys. Fluids. Click here to see the version of record.

perturbation velocity field at the first correction

$$\tilde{v}_z^{(1)} = D_3 \exp^{[-kz]}[1 - \frac{4k^3W(\iota+W)zRe^{1/2}}{2Wc^{(0)}k^3(2\iota-(c^{(0)}))^2+2W}]+$$
$$D_4 \exp^{[kz]}[1 - \frac{4k^3W(\iota-W)zRe^{1/2}}{2Wc^{(0)}k^3(2\iota+(c^{(0)}))^2-2W}]+$$
$$D_2 exp^{[-\iota kW+k\Theta]z}$$
$$[1 + \frac{\iota Re^{1/2}(\iota c^{(0)}k^3((c^{(0)})^2-2W)W+2c^{(0)}c^{(1)}k^4W^2((c^{(0)})^2+2\iota\Theta)z)}{2k^3W(2+2W^2+(c^{(0)})^2(-2W-\iota\Theta))}]$$
$$+ D_1 exp^{[-\iota kW-k\Theta]z}$$
$$[1 + \frac{Re^{1/2}(\iota c^{(0)}k^3((c^{(0)})^2-2W)W+2c^{(0)}c^{(1)}k^4W^2((c^{(0)})^2-2\iota\Theta)z)}{2k^3W(-2\iota(1+W^2)+(c^{(0)})^2(2\iota W+\Theta))}]$$
$$- D_2[\frac{2c^{(0)}exp^{[-\iota kW+k\Theta]z}Re^{1/2}k^4W^2[(c^{(0)})^2+2\iota\Theta]}{-4\iota k^3W+4\iota(c^{(0)})^2k^3W^2-4\iota k^3W^3-2(c^{(0)})^2k^3W\Theta}]$$
$$[\frac{z^2}{2} - \frac{(4k^2-5(c^{(0)})^2k^2W+4k^2W^2-6\iota k^2W(c^{(0)})^2(2\iota W+\Theta))z}{-4\iota k^3W+4\iota(c^{(0)})^2k^3W^2-4\iota k^3W^3-2(c^{(0)})^2k^3W\Theta}]$$
$$- D_1[\frac{2c^{(0)}exp^{[-\iota kW-k\Theta]z}Re^{1/2}k^4W^2[(c^{(0)})^2-2\iota\Theta]}{-4\iota k^3W+4\iota(c^{(0)})^2k^3W^2-4\iota k^3W^3+2(c^{(0)})^2k^3W\Theta}]$$
$$[\frac{z^2}{2} - \frac{(4k^2-5(c^{(0)})^2k^2W+4k^2W^2+6\iota k^2W(c^{(0)})^2(2\iota W+\Theta))z}{-4\iota k^3W+4\iota(c^{(0)})^2k^3W^2-4\iota k^3W^3+2(c^{(0)})^2k^3W\Theta}]. \quad (61)$$

where Θ is defined as $[\Theta = \sqrt{1-(c^{(0)})^2W+W^2}]$.

The governing equations at first correction terms for the deformable solid are obtained using asymptotic series expansions of the displacement and pressure fields, Eqs. 37-39, in linearized governing equations, Eqs. 14a-14c. After separating, we get following equations for the deformable solid

$$d_z\tilde{u}_z^{(1)} + ik\tilde{u}_x^{(1)} = 0, \quad (62)$$
$$-ik\tilde{p}_g^{(1)} + \frac{1}{\Gamma}(d_z^2-k^2)\tilde{u}_x^{(1)} = -k^2(c^{(0)})^2\tilde{u}_x^{(1)} - 2c^{(0)}c^{(1)}k^2\tilde{u}_x^{(0)}, \quad (63)$$
$$-d_z\tilde{p}_g^{(1)} + \frac{1}{\Gamma}(d_z^2-k^2)\tilde{u}_z^{(1)} = -k^2(c^{(0)})^2\tilde{u}_z^{(1)} - 2c^{(0)}c^{(1)}k^2\tilde{u}_z^{(0)}. \quad (64)$$

We obtained a 4^{th}- order nonhomogeneous differential equations for the deformable solid by combining Eqs. 62-64

$$[d_z^2-k^2][d_z^2-k^2+k^2\Gamma(c^{(0)})^2]\tilde{u}_z^{(1)} = 2ic^{(0)}c^{(1)}k^3\Gamma d_z\tilde{u}_x^{(0)} - 2c^{(0)}c^{(1)}\Gamma k^4\tilde{u}_z^{(0)}. \quad (65)$$

By comparing Eq. 43 with Eq. 65, we find that the differential operator operating on $\tilde{u}_z^{(0)}$ is identical to the one operating on $\tilde{u}_z^{(1)}$. The analytical solution of the above equation gives first correction

displacement field $\tilde{u}_z^{(1)}$

$$\tilde{u}_z^{(1)} = C_1 \exp^{[kz]}(1 + \frac{4c^{(0)}c^{(1)}\Gamma k^4 z}{2(c^{(0)})^2\Gamma k^3}) + C_2 \exp^{[-kz]}(1 + \frac{4c^{(0)}c^{(1)}\Gamma k^4 z}{-2(c^{(0)})^2\Gamma k^3}) +$$
$$C_3(\exp^{[-\iota kW + k\xi]z} + \exp^{[-kz\xi]} \frac{4c^{(0)}c^{(1)}\Gamma k^4 z}{2(c^{(0)})^2\Gamma k^3 \xi} - \exp^{[-kz\xi]} \frac{2(c^{(0)})^3 c^{(1)}\Gamma^2 k^4 z}{2(c^{(0)})^2\Gamma k^3 \xi}) +$$
$$C_4(\exp^{[-\iota kW - k\xi]z} + \exp^{[kz\xi]} \frac{4c^{(0)}c^{(1)}\Gamma k^4 z}{-2(c^{(0)})^2\Gamma k^3 \xi} - \exp^{[kz\xi]} \frac{2(c^{(0)})^3 c^{(1)}\Gamma^2 k^4 z}{-2(c^{(0)})^2\Gamma k^3 \xi}). \quad (66)$$

where ξ is defined as $\xi = \sqrt{1 - (c^{(0)})^2\Gamma}$.
The governing equations at first correction are solved using following boundary and interface conditions

$$\tilde{v}_z^{(1)} = \tilde{v}_x^{(1)} = 0 \quad at \quad z = 1, \quad (67)$$
$$\tilde{u}_z^{(1)} = \tilde{u}_x^{(1)} = 0 \quad at \quad z = -H, \quad (68)$$

Interface conditions:

$$\tilde{v}_z^{(1)} = -ikc^{(0)}\tilde{u}_z^{(1)} - ikc^{(1)}\tilde{u}_z^{(0)}, \quad (69)$$
$$\tilde{v}_x^{(1)} + \tilde{u}_z^{(0)} = -ikc^{(0)}\tilde{u}_x^{(1)} - ikc^{(1)}\tilde{u}_x^{(0)}, \quad (70)$$
$$\tilde{\tau}_{xz}^{(1)} - 2ikW\tilde{u}_z^{(1)} = \frac{1}{\Gamma}(d_z\tilde{u}_x^{(1)} + ik\tilde{u}_z^{(1)}), \quad (71)$$
$$-\tilde{p}_f^{(1)} + \tilde{\tau}_{zz}^{(1)} = -\tilde{p}_g^{(1)} + \frac{2}{\Gamma}d_z\tilde{u}_z^{(1)}. \quad (72)$$

The set of linearized equations for leading order and first correction asymptotic analysis are solved using Mathematica. The wavespeed and displacement fields obtained by leading order analysis are then used to calculate the first correction to the wavespeed.

D. No-flow asymptotic analysis

In this section, we perform an asymptotic analysis of the shear waves in the coupled viscoelastic fluid-solid system in the absence of flow. In this limit, the flow velocity scale is no longer relevant, and the leading order governing equations are rescaled to eliminate velocity. Earlier study by Shankar and Kumar[18] showed that, in $Re \ll 1$ limit the leading order wavespeed for the UCM plane Couette flow is purely real. However, for the same $Re \ll 1$ limit, the leading order asymptotic analysis for UCM plane Couette flow past a deformable solid results in a complex wavespeed. The motivation to conduct the no-flow analysis is to understand whether the of presence of a deformable wall is enough for complex wavespeed of shear waves, or if flow is equally important. In this section, we consider $W = \Gamma$ for the sake of simplicity, although the conclusions are valid in general.

Because V is no longer a relevant velocity scale in the absence of flow, the leading order linearized governing equations for the fluid, Eqs. 29-34, and the deformable solid, Eqs. 40-42, are rescaled using the following nondimensionalization scheme: $\sqrt{\frac{\eta}{\lambda\rho}}$ for velocity, G or η/λ for stress and pressure, R for length and $R/\sqrt{\frac{\eta}{\lambda\rho}}$ for time. The resulting no-flow leading order equations for

This manuscript was accepted by Phys. Fluids. Click here to see the version of record.

fluid are

$$d_z\tilde{v}_z^{(0)} + ik\tilde{v}_x^{(0)} = 0, \tag{73}$$
$$-ik\tilde{c}\tilde{\tau}_{zz}^{(0)} = 2d_z\tilde{v}_z^{(0)}, \tag{74}$$
$$-ik\tilde{c}\tilde{\tau}_{xz}^{(0)} = d_z\tilde{v}_x^{(0)} + ik\tilde{v}_z^{(0)} \tag{75}$$
$$-ik\tilde{c}\tilde{\tau}_{xx}^{(0)} = 2ik\tilde{v}_x^{(0)}, \tag{76}$$
$$ik\tilde{p}_f^{(0)} = ik\tilde{\tau}_{xx}^{(0)} + d_z\tilde{\tau}_{xz}^{(0)} + ik\tilde{c}\tilde{v}_x^{(0)}, \tag{77}$$
$$ik\tilde{c}\tilde{v}_z^{(0)} = d_z\tilde{p}_f^{(0)} + ik\tilde{\tau}_{xz}^{(0)} + d_z\tilde{\tau}_{zz}^{(0)}, \tag{78}$$

whereas the leading order equations for the deformable solid are

$$-k^2\tilde{c}^2\tilde{u}_x^{(0)} = -ik\tilde{p}_g^{(0)} + (d_z^2 - k^2)\tilde{u}_x^{(0)}, \tag{79}$$
$$-k^2\tilde{c}^2\tilde{u}_z^{(0)} = -d_z\tilde{p}_g^{(0)} + (d_z^2 - k^2)\tilde{u}_z^{(0)}, \tag{80}$$
$$d_z\tilde{u}_z^{(0)} + ik\tilde{u}_x^{(0)} = 0. \tag{81}$$

Similarly, boundary and interface conditions for the no-flow analysis are also rescaled using the same nondimensionalization scheme. At the boundaries, no slip and no penetration conditions are applicable which takes the following form

$$\tilde{v}_z^{(0)} = \tilde{v}_x^{(0)} = 0 \quad at \quad z = 1, \tag{82}$$
$$\tilde{u}_z^{(0)} = \tilde{u}_x^{(0)} = 0 \quad at \quad z = -H, \tag{83}$$

whereas the interface conditions are given by

$$\tilde{v}_z^{(0)} = -ik\tilde{c}\tilde{u}_z^{(0)} \tag{84}$$
$$\tilde{v}_x^{(0)} = -ik\tilde{c}\tilde{u}_x^{(0)} \tag{85}$$
$$\tilde{\tau}_{xz}^{(0)} = d_z\tilde{u}_x^{(0)} + ik\tilde{u}_z^{(0)}, \tag{86}$$
$$-\tilde{p}_f^{(0)} + \tilde{\tau}_{zz}^{(0)} = -\tilde{p}_g^{(0)} + d_z\tilde{u}_z^{(0)}. \tag{87}$$

The leading order governing equations for both the fluid and the solid can be simplified to yield the following 4^{th}- order ODEs. It turns out that both the ODEs are identical for the case when $W = \Gamma$

$$[d_z^2 - k^2][d_z^2 - k^2(1 - \tilde{c}^2)]\tilde{v}_z^{(0)} = 0, \tag{88}$$
$$[d_z^2 - k^2][d_z^2 - k^2(1 - \tilde{c}^2)]\tilde{u}_z^{(0)} = 0, \tag{89}$$

where, $\tilde{c} \Leftarrow c^2 ReW$. The analytical solution of the above Eqs. 88-89, are given by

$$\tilde{v}_z^{(0)} = M_1 \exp^{[kz]} + M_2 \exp^{[-kz]} + M_3 \exp^{[k\sqrt{1-(\tilde{c}^{(0)})^2}]z} + M_4 \exp^{[-k\sqrt{1-(\tilde{c}^{(0)})^2}]z}, \tag{90}$$

$$\tilde{u}_z^{(0)} = N_1 \exp^{[kz]} + N_2 \exp^{[-kz]} + N_3 \exp^{[k\sqrt{1-(\tilde{c}^{(0)})^2}]z} + N_4 \exp^{[-k\sqrt{1-(\tilde{c}^{(0)})^2}]z}. \tag{91}$$

Numerical values of the wavespeed for the no-flow analysis are obtained using Mathematica. The method used to calculate the results is the same as discussed at the end of Sec. II-B.

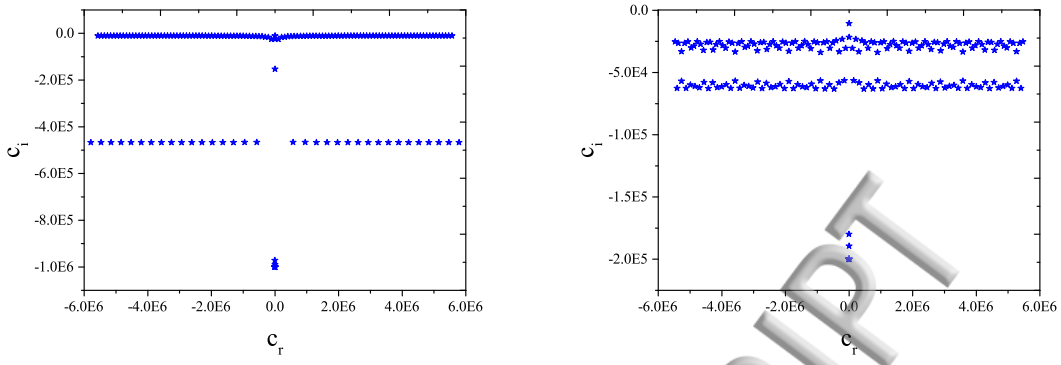

(a)$W = 10^{-6}$

(b)$W = 5 \times 10^{-6}$

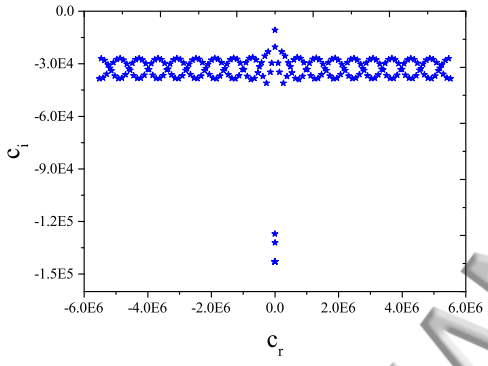

(c)$W = 7 \times 10^{-6}$

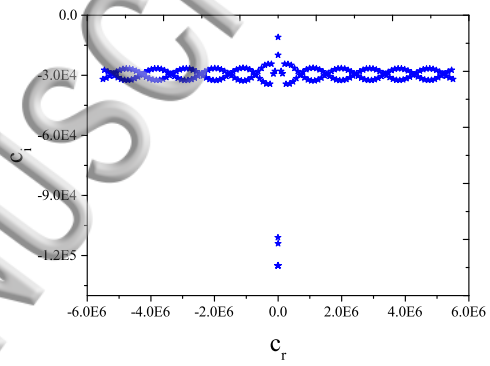

(d)$W = 8 \times 10^{-6}$

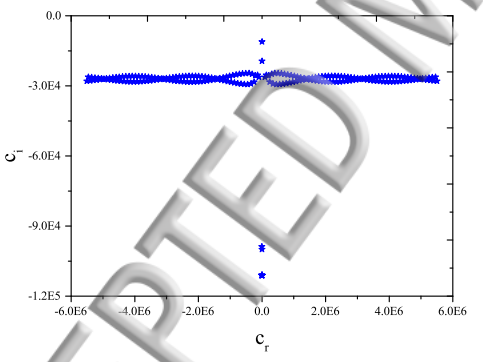

(e)$W = 9 \times 10^{-6}$

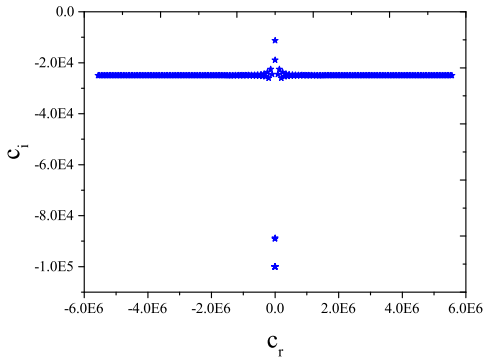

(f)$W = 10^{-5}$

FIG. 2: Eigenspectra for plane Couette flow past a deformbale wall demonstrating the resonance phenomenon: Data for $Re = 10^{-4}$, $\Gamma = 10^{-5}$, $H = 1$, and $k = 1$. Spectra shown for different W as indicated in panels (a)-(f).

III. RESULTS AND DISCUSSION

A. Resonance of shear waves

In the limit of Reynolds number $Re \ll 1$, the numerical results from the spectral method clearly demonstrate the effect of Γ and W on the HFGL as well as solid eigenmodes. It is useful here to

first recall that both the UCM (viscoelastic) fluid and the linear elastic solid support shear waves in isolation, with the only difference that in the fluid, the shear waves are damped out eventually due to dissipative effects in the viscoelastic fluid. Thus, it is possible to identify the shear waves in the fluid and the elastic solid in the limit when the deformable solid approaches the rigid limit $\Gamma \to 0$, or when the fluid is only slightly elastic, i.e. $W \to 0$. The eigenspectra shown in figure 2 yield some insight into the mechanism of interaction of the deformable solid and viscoelastic fluid via the interface. When both Γ and W are very small, the shear waves corresponding to the fluid and the solid are well separated, and are nearly independent of each other. For instance, in Fig. 2(a), the class of modes with $c_i = -1/(2kW) = 5 \times 10^4$ (for $W = 10^{-6}, k = 1$) represent the shear waves (referred to as HFGL modes in this paper) of the viscoelastic fluid, while the class of modes with a lower decay rate correspond to the shear waves in the elastic solid. The shear waves in a purely elastic solid (that is not adjacent to a viscous fluid) are not damped, but the shear waves of the elastic solid adjacent to the fluid are damped due to dissipative effects in the fluid, whether it is Newtonian or viscoelastic. It also suggests that as we gradually increase either W or Γ (i.e. either by making the fluid more elastic or the solid more elastic), the eigenspectra of the fluid and solid move towards each other. It is easy to understand the movement of the HFGL line as W is increased, since they are characterized by $c_i = -1/(2kW)$. The increase in decay rate (i.e. the downward movement) of the damped shear waves in the solid can also be understood as follows: the timescale for decay of fluctuations in a coupled fluid-solid system is η/G, where η is the viscosity of the fluid and G is the shear modulus of the elastic solid. As W is increased at fixed Γ, $W/\Gamma = \lambda/(\eta/G)$ increases, implying that the viscous fluid-elastic solid relaxation time (η/G) decreases compared to the fluid relaxation time λ. To illustrate the phenomena, we fixed Γ and varied W while keeping rest of the parameters constant. As we gradually increase W from 10^{-6} to 10^{-5}, the decay rate of the solid eigenmodes increases whereas the decay rate of the fluid eigenmodes decreases as shown in Fig. 2(a)–2(e). It can be seen in Fig. 2(e) that both fluid and solid spectra merge and the decay rate of the merged eigenspectra is given by

$$c_i = \frac{-1}{2k(W+\Gamma)} \tag{92}$$

which suggests that both W and Γ (i.e. fluid and solid elasticity) have a combined effect on the shifting and merging of the two eigenspectra. It is interesting to note that when $\Gamma \to 0$, this expression approaches $c_i = -1/(2kW)$ corresponding to the decay rates of HFGL modes, while when $W \to 0$, it reduces to $c_i = -1/(2k\Gamma)$ corresponding the decay rates of shear waves in an elastic solid adjacent to a viscous liquid.

Figure. 2(f) shows the condition when both Γ and W are equal and both the fluid and the solid eigenspectra merge. At this point, the shear waves in the fluid and the solid have identical decay rates which further suggests that the fluid and solid eigenmodes are indistinguishable and the coupled system behaves as a single composite material. In their work, Kumar and Shankar[22] showed the effect of wall deformability on HFGL modes for a given W using a leading order asymptotic analysis. Their analysis showed that the coupled system is unstable at very low Γ value, but they could not capture all the eigenmodes. This motivated us to revisit the study using the spectral method. The condition at which both the fluid and solid eigenmodes are indistinguishable occurs when the $W/\Gamma = 1$ and both the fluid and solid shear waves resonate in this regime.

It can be inferred from figs. 2 and 3 that with an increase in W, the decay rate of perturbations in the fluid decrease. On the other hand the decay rate of disturbances in deformable solid increases. It suggests that the increase in W has a destabilizing effect on the fluid HFGL modes while it stabilizes the solid eigenmodes. Further increase in either W or Γ beyond a critical value may

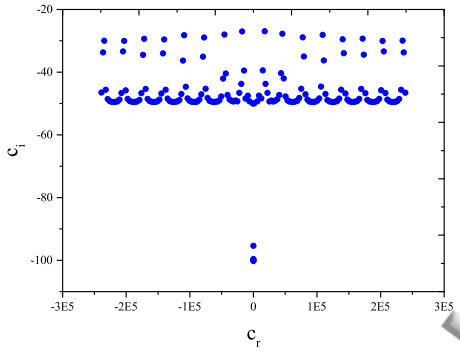

FIG. 3: Eigenspectrum for plane Couette flow past a deformbale wall at $Re = 10^{-4}$, $\Gamma = 10^{-4}$, $W = 10^{-2}$, $H = 1$, and $k = 1$.

introduce an instability in the system as reported by Kumar and Shankar[22]. In other words, the dimensional wave speed for UCM fluid in rigid channel is proportional to $(\frac{\eta}{\rho\lambda})^{1/2}$ whereas, the wave speed for deformable solid proportional to $(\frac{G}{\rho})^{1/2}$. When both the wave speeds of fluid and solid disturbances are equal, the ratio of $\frac{W}{\Gamma}$ is 1 and therefore disturbances travelling in both solid and fluid have the same frequency and resonance occurs. Once resonance is achieved, a further increase in the value of Γ or W leads to increase in c_i of the resonated eigenmodes.

Our analysis hence confirms that the instability predicted by Kumar and Shankar[22], is indeed caused due to a resonance between the shear waves in the viscoelastic fluid and elastic solid. It is therefore appropriate to refer to this as a 'resonant' instability, since the instability emerges after a resonance of the underlying shear waves in the fluid and solid. It can also be inferred from Fig. 2(f) that, at the onset of resonance, the qualitative behaviour of the eigenspectra of plane Couette flow of UCM fluid past a linear elastic solid is different from that of plane Couette flow of UCM fluid in the rigid channel. The eigenspectrum shown in Fig. 3 suggests that when W is large compared to Γ, the HFGL eigenmodes start 'pinching' up while the solid eigenmodes start appearing in the eigenspectrum. A further increase in Γ leads to more and more solid eigenmodes to appear in the eigenspectrum with a wavespeed similar to the wavespeed of fluid disturbances. When Γ and W are equal as shown in Fig. 2(f), both the fluid and solid shear waves resonate and all eigenmodes have same decay rate as explained above.

B. First correction

Gorodtsov and Leonov[20] first performed asymptotic analysis for UCM plane Couette flow through a rigid channel in $Re \ll 1$ limit. They concluded that the flow is unstable and the instability arises due to the viscoelastic nature of the fluid. They analytically calculated the decay rate of perturbations and showed the condition of instability. However, later Renardy and Renardy[21] performed numerical analysis for the same flow system and found that the plane Couette flow of UCM fluid is linearly stable for all Reynolds numbers. As shown by Kumar and Shankar[22], the leading order asymptotic analysis of the plane Couette flow in a rigid channel yields a real wave speed and hence the first correction to the wave speed is obtained to theoretically predict the stability of plane Couette flow. Table I shows a comparison of the least stable eigenvalues obtained from the leading order asymptotic analysis, from our numerical analysis using spectral method,

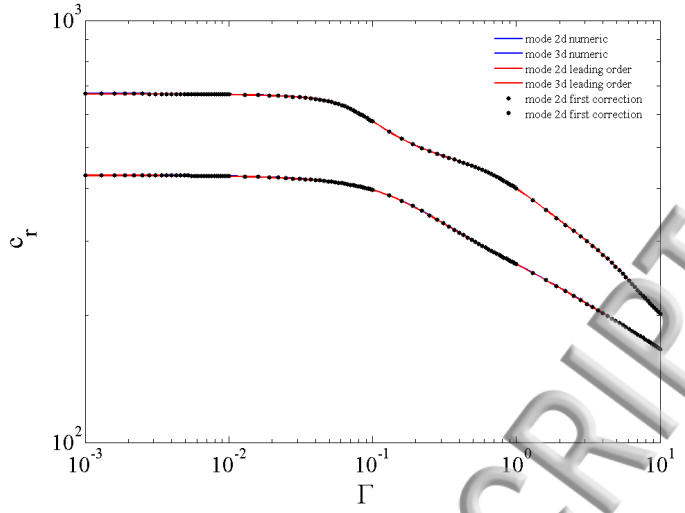

FIG. 4: c_r vs Γ curve comparing numeric and asymptotic results obtained at $Re = 10^{-4}$, $W = 2$, $H = 1$, and $k = 1$

and from the asymptotic analysis correct up to the first correction to the wave speed. The results obtained by the first correction shows an excellent agreement with the numerical (spectral) results and hence the stability of the system can be analytically predicted.

Kumar and Shankar[22] also performed the asymptotic analysis in the low Reynolds number limit with $W \sim O(1)$ for stability of UCM plane Couette flow past a deformable solid. They showed that the real part of the wavespeed obtained at the leading order in the asymptotic analysis agrees with the one obtained using numerical approach over the entire range of Γ. However, the imaginary part of the wave speed is not in good agreement with the numerically obtained wavespeed for small Γ. Nevertheless, for comparatively large values of Γ, the leading order analysis accurately predicts the stability of the system. In this work, we obtained the first correction to the wave speed for flow past flexible surface in order to theoretically predict the stability of the flow system. The results shows that the wavespeed obtained by asymptotic approach up to first correction agree well with the numerically obtained wavespeed for the entire range of Γ.

Figure 4 shows a comparison of c_r values obtained from the numerical solution with c_r values obtained from leading order and first correction asymptotic analysis. Similarly, Fig. 5 compares c_i values obtained by both numerical as well and asymptotic approaches. It can be inferred from these figures that the results obtained by asymptotic analysis up to the first correction are in an excellent agreement with the numerical results. The comparison suggests that the first correction has a stabilizing effect on the system as shown in fig. 4 for low Γ. Table II lists the least stable eigenmodes for the UCM plane Couette flow past a deformable solid obtained by numerical and asymptotic approaches to support the aforementioned claim of prediction of the stability of the coupled flow system.

C. No-flow calculation

In this section, we analytically calculate the coupled shear waves in the absence of flow, in order to demonstrate the importance of the flow on the growth of the disturbances. The results obtained are then compared with the results of first correction asymptotic analysis to draw the conclusions. However, the no-flow analysis is carried out for both UCM plane Couette flow in a rigid channel

This manuscript was accepted by Phys. Fluids. Click here to see the version of record.

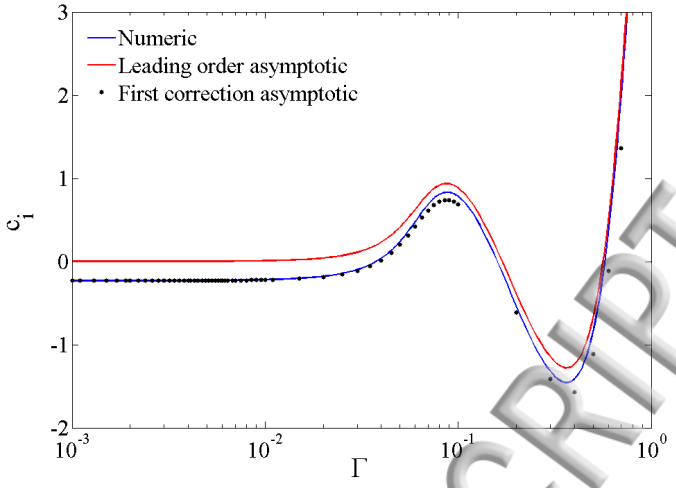

FIG. 5: c_i vs Γ curve comparing numeric and asymptotic results obtained at $Re = 10^{-4}$, $W = 2$, $H = 1$, and $k = 1$

TABLE I: Least stable eigenmodes for plane Couette flow in rigid channel

plane Couette flow, $Re = 10^{-4}$, $k = 1$, $W = 2$				
Asymptotic leading order	Numerical results		Asymptotic first correction	
c_r	c_r	c_i	c_r	c_i
± 226.768	± 226.766927	$-0.34248965i$	± 226.766927	$-0.34248965i$
± 354.169	± 354.168896	$-0.28006144i$	± 354.169183	$-0.28006155i$
± 569.414	± 569.413926	$-0.25785959i$	± 569.414044	$-0.25785948i$
± 787.805	± 787.805263	$-0.25371763i$	± 787.805323	$-0.25371761i$
± 1007.74	± 1007.74238	$-0.25218279i$	± 1007.74242	$-0.25218278i$

and for UCM flow past a deformable surface in $Re \ll 1$ limit for arbitrary W. Table III shows a comparison of the eigenmodes thus obtained by leading order asymptotic analysis results for the no-flow case in a rigid channel, with the numerical results when the flow is switched on. The comparison shows that the eigenmodes for the no-flow case are purely real. But the real parts of the wavespeeds with flow are very similar to those without flow. Thus, even in the presence of flow, to leading order, the flow does not affect the leading order eigenvalue calculation. Physically, this implies that to leading order, the fluid appears to be static in the asymptotic analysis. These eigenmodes belong to the UCM fluid are termed as fluid modes. We next extended the above analysis (in the absence of flow) to a deformable channel. The equations $(79 - 81)$ govern the dynamics of the system. On comparing the Eq. 88 with 89, it turns out that the linear differential operator operating on $\tilde{v}_z^{(0)}$ is identical to the one operating on $\tilde{u}_z^{(0)}$. It can be inferred from the comparison that identical differential operators result in qualitatively identical eigenmodes and

TABLE II: Eigenvalues for Couette flow past a deformable solid

$Re = 10^{-4}$, $W = 2$, $k = 1$, $\Gamma = 10^{-3}$				$Re = 10^{-4}$, $W = 0.01$, $k = 1.5$, $\Gamma = 10^{-2}$			
Numerical results		Asymptotic first correction		Numerical results		Asymptotic first correction	
c_r	c_i	c_r	c_i	c_r	c_i	c_r	c_i
330.484	$-0.256532i$	330.484	$-0.256718i$	7298.28	$-16.1518i$	7298.38	$-16.1519i$
682.270	$-0.198504i$	682.270	$-0.198716i$	3066.54	$-15.2690i$	3066.74	$-15.2721i$
1024.63	$-0.194547i$	1024.63	$-0.194774i$	5190.97	$-16.1400i$	5191.06	$-16.1405i$
-1707.01	$-0.193134i$	-1707.01	$-0.193401i$	-2042.02	$-15.7882i$	-2042.29	$-15.7903i$

TABLE III: Eigenmodes for plane Couette flow in rigid channel

plane Couette flow, $Re = 10^{-4}$**,** $k = 1$**,** $W = 2$			
Leading order no-flow results		Numerical results with flow	
c_r	c_i	c_r	c_i
6214.753	6.81682×10^{-14}	6214.052	-50.00045
9006.041	2.33191×10^{-15}	9006.402	-49.99979
12532.37	1.29396×10^{-13}	12532.77	-50.00010
15462.66	5.34015×10^{-14}	15462.08	-49.99992
18827.97	8.48822×10^{-16}	18827.41	-50.00004
21816.14	1.34815×10^{-13}	21816.58	-49.99996
25115.83	7.08482×10^{-14}	25116.28	-50.00002

these are termed as solid eigenmodes. Kumar and Shankar[22] have performed leading order analysis for UCM plane Couette flow and showed that the fluid eigenmodes are purely real even in the presence of flow in a rigid channel. The major goal of no-flow analysis is to see whether the presence of a deformable wall alone is the only reason for the complex wave speed and for the instability reported by Kumar and Shankar[22], and to examine whether flow is an equal contributor to the instability. To answer this question the leading order linearized governing equations for the flow past deformable wall are rescaled to get no-flow equations (refer Eqs. 73-87). Table IV shows

TABLE IV: Eigenmodes for plane Couette flow past a deformbale wall

$Re = 10^{-4}$**,** $k = 1.2$**,** $H = 1$**,** $W = 10^{-2}$ **and** $\Gamma = 10^{-2}$			
No-flow leading order results		Numerical results with flow	
c_r	c_i	c_r	c_i
2537.249	1.64755×10^{-13}	2537.248	21.49573
3797.324	5.78594×10^{-14}	3797.330	19.32641
5198.085	2.46021×10^{-14}	5198.314	20.83956
6468.128	8.99615×10^{-14}	6468.240	20.31331
7828.982	1.08180×10^{-13}	7829.217	20.85436
9108.264	2.42736×10^{-14}	9108.413	20.30691

a comparison of the data obtained by solving the leading order no-flow equations with the results obtained by the numerical solution.

The leading order asymptotic analysis for plane Couette flow system, when the flow is absent, shows that the eigenvalues are purely real at leading order. This suggests that the static viscoelastic fluid-deformable solid problem is neutrally stable at leading order. Kumar and Shankar[22] performed leading order asymptotic analysis and showed that the system is unstable in $Re \ll 1$ limit. Comparison of the data obtained by no flow calculations with numerical results shows that even in the presence of a deformable wall and nonzero normal stress difference in in the no-flow analysis, the imaginary part of the wave speed is absent. In other words, when the flow is turned off, to leading order in the asymptotic analysis, the fluid will appear to be a static elastic solid and the coupled flow system effectively reduces to a single linear elastic solid with shear waves with wavespeed proportional to $\frac{\eta}{\lambda G}$. It can be inferred from table IV that even if the wall is deformable, the eigenmodes obtained are purely real and in the absence of flow the system is neutrally stable. We can thus conclude that the flow is mandatory for the resonance of shear waves and instability in the system. Particularly, as we switch on the flow, shear waves of both the fluid and the solid resonate to give rise a purely flow-driven instability. Kumar and Shankar[22] have shown that in the leading order c_i scales as Γ^2 for a given W and showed the effect of flow on the growth rate. Here, we have examined the effect of flow on c_i for a particular Γ by varying W. Figure 6 shows that c_i is proportional to W^2, which suggests that the growth rate of disturbances is highly dependent on the flow. Hence, it can be said that in the absence of flow the wave speed is purely real and

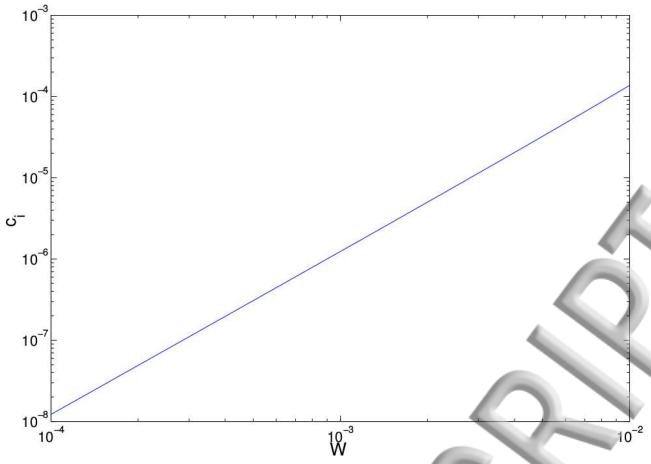

FIG. 6: c_i vs W showing the scaling of c_i w.r.t W at $Re = 10^{-6}$, $W = 10^{-4}$ to 10^{-2}, $\Gamma = 1$, $H = 1$, and $k = 1$.

there is no resonant instability of fluid and solid shear waves. Thus, the imposed flow is crucial in destabilizing the resonant shear waves in the coupled fluid-solid system.

D. Effect of Re on resonance

In the above section, we discussed the phenomenon of resonance where we fixed rest of the parameters while smoothly varying W. In this section, we address the question of how inertial forces affect the resonance. To this end, we slowly varied the Reynolds number while keeping rest of the parameters fixed and observed the eigenspectra. Both W and Γ are fixed at 10^{-2}, whereas the nondimensional solid thickness $H = 1$. Figures 7 and 8 show there is no qualitative change in the eigenspectrum when we increase Re from 10^{-2} to 10^{-1}. However, the range of the wavespeed, c_r, is decreased by an order of the magnitude. A further increase in Re from 10^{-1} to 1 as shown in the fig. 9 suggests that de-coupling of the resonated eigenspectrum happens at higher Re. In other words, when the inertia is sufficiently large compared to the W and Γ, the resonated eigenspectra decouples and both fluid and solid disturbances decay with different rates. It can be inferred from the above discussion that for the resonance to occur, the Reynolds number must be small or comparable to the W and Γ values, and fluid inertia destroys the resonance.

E. Effect of H on the resonant eigenspectrum

The non-dimensional solid thickness H also plays a major role on the stability of coupled flow systems. In this section, we examined the effect of H on the resonant eigenspectra. Kumar and Shankar[18] showed that UCM plane Couette flow past a linear elastic solid becomes unstable even in the creeping flow limit at sufficiently high value of H. This suggests that the deformable solid has a destabilizing effect. Figure 10 shows the eigenspectrum for the UCM plane Couette flow past a linear elastic solid at $W = \Gamma = 10^{-2}$ and $Re = 10^{-4}$ for $H = 0.1$. The figure shows that the c_i value for the resonated eigenspectrum is much lower than predicted by equation (92) which suggests a stabilizing effect. However, it is important to note that the variation of H from 1

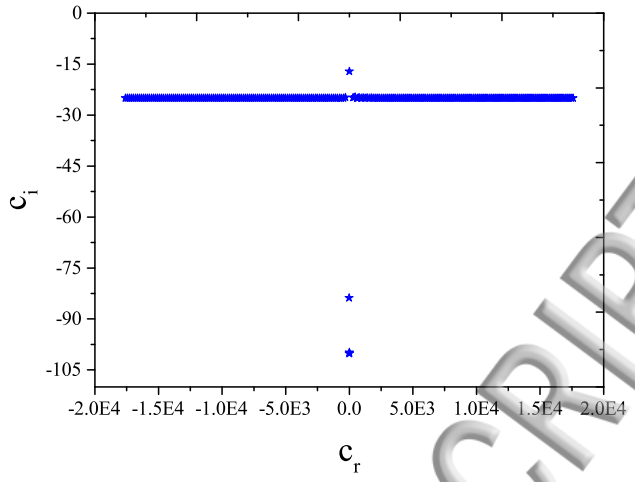

FIG. 7: Eigenspectrum for plane Couette flow past a deformbale wall at $Re = 10^{-2}$, $\Gamma = 10^{-2}$, $W = 10^{-2}$, $H = 1$, and $k = 1$.

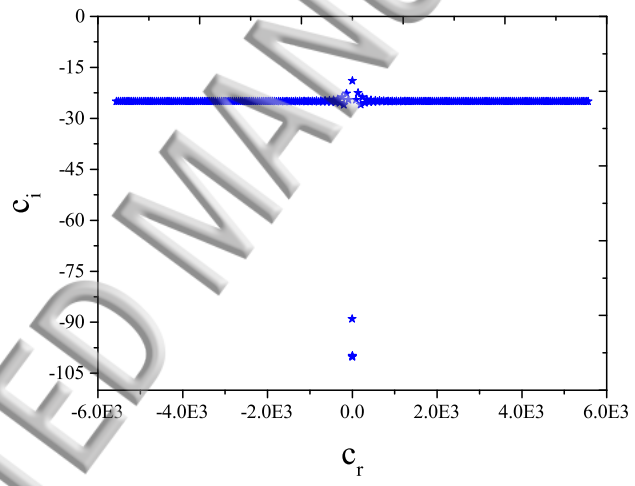

FIG. 8: Eigenspectrum for plane Couette flow past a deformbale wall at $Re = 10^{-1}$, $\Gamma = 10^{-2}$, $W = 10^{-2}$, $H = 1$, and $k = 1$.

to 0.1 is not eliminating the phenomenon of resonance. On the other hand, fig. 9 shows lowering of decay rate c_i when H is increased to 10. As expected, increase in the solid thickness has a destabilizing effect on the coupled flow system. It is again important to note that the increase in H is not removing the phenomenon of resonance. Nevertheless, both increase and decrease in solid thickness from $H = 1$ is introducing a wavy pattern near the centre of the symmetric eigenspectrum.

In addition to the effect of H on the resonant eigenspectrum, we show the structure of an eigenspectrum when the $\frac{W}{\Gamma} \neq 1$. Figure 12 displays an eigenspectrum for the coupled flow system when the $\frac{W}{\Gamma}$ ratio is 0.1. The condition of resonance is not achieved yet but at $\frac{W}{\Gamma} \geq 0.1$ both solid modes and HFGL modes start merging as shown in the fig. 13. Similarly, fig. 13 shows an eigenspectrum for $\frac{W}{\Gamma} = 10$. It can be inferred from the eigenspectra that when the $\frac{W}{\Gamma}$ ratio is

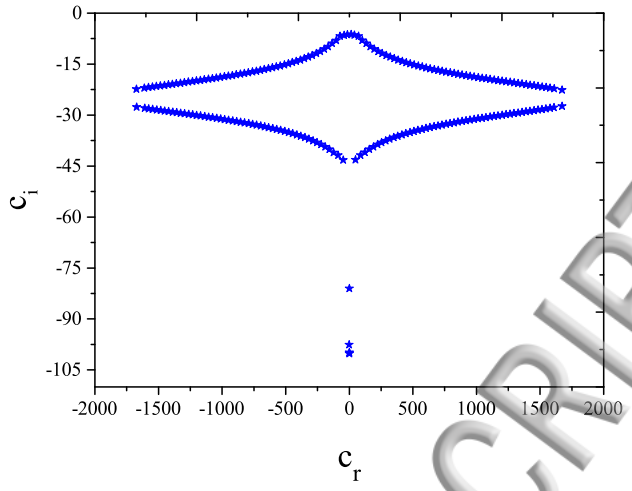

FIG. 9: Eigenspectrum for Couette flow past a deformbale wall at $Re = 1$, $\Gamma = 10^{-2}$, $W = 10^{-2}$, $H = 1$, and $k = 1$.

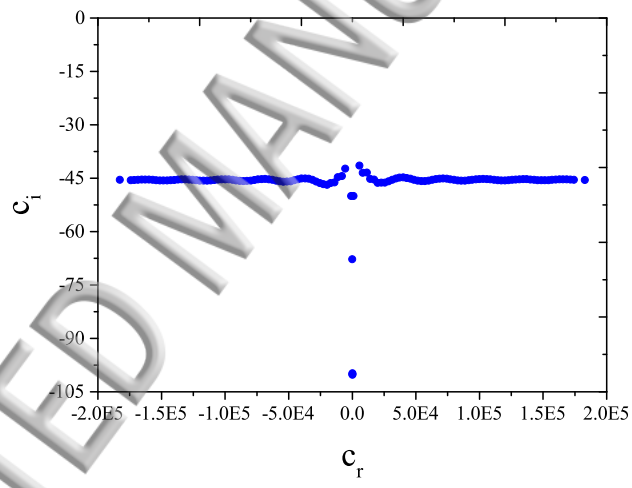

FIG. 10: Eigenspectrum for plane Couette flow past a deformbale wall at $Re = 10^{-4}$, $\Gamma = 10^{-2}$, $W = 10^{-2}$ and $k = 1$ at $H = 0.1$.

greater than 1 the system is highly stable. On the other hand, if the ratio is less than 1 the coupled flow system is less stable. When W and Γ are not equal, but are of the same order of magnitude, this interaction of HFGL and solid eigenmodes occurs as suggested in Figs. 12 and 13.

Before we conclude, it is pertinent to provide some dimensional estimates of the physical parameters for which this instability can be observed in experiments. To this end, we consider the dimensionless parameters $\Gamma \sim 0.1$, $W \sim 1$ and $Re \sim 1$. Typical shear moduli of soft elastomers (prepared using polydimethyl siloxane) used in previous experiments[4,29] are in the range 10^4 Pa, and for concentrated polymer solutions (of say polyacrylamide in glycerine-water solvent) we choose $\eta \sim 1$ Pa s, thus yielding $V/R \sim 10^3$ s^{-1}. If we set $W \sim 1$, then this yields $\tau_R \sim 0.001$s, and using $Re \sim 1$, we obtain $R \sim 1$ mm and $V = 1$ m/s. Thus, the instabilities predicted in this study can be potentially observed in the flow of concentrated polymer solutions through microscale

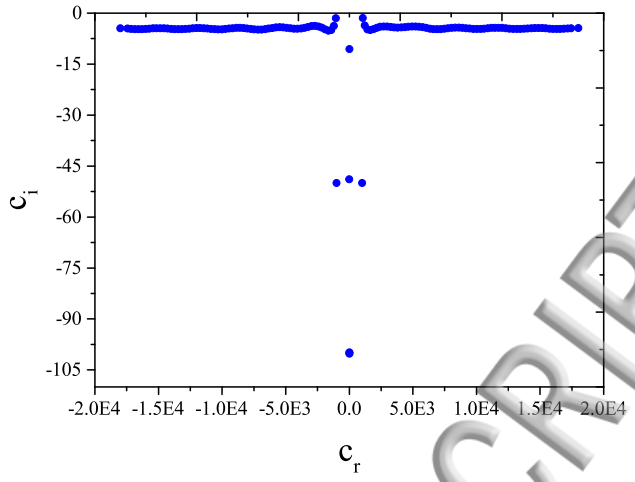

FIG. 11: Eigenspectrum for plane Couette flow past a deformbale wall at $Re = 10^{-4}$, $\Gamma = 10^{-2}$, $W = 10^{-2}$ and $k = 1$ at $H = 10$.

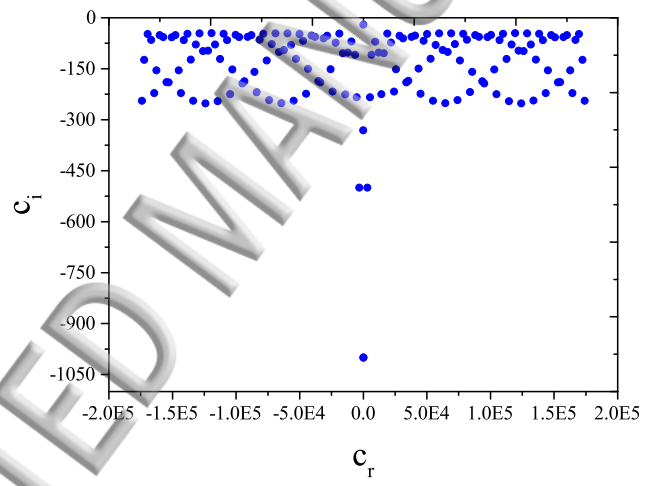

FIG. 12: Eigenspectrum for plane Couette flow past a deformbale wall at $Re = 10^{-4}$, $W = 10^{-3}$, $\Gamma = 10^{-2}$, $k = 1$, $H = 1$, at $\frac{W}{\Gamma} = 0.1$.

geometries with deformable walls. It is also worth emphasizing that while the present results are confined to the UCM model, which does not have a solvent contribution in the model, while the Oldroyd-B model accounts for the same. Our earlier work[22] had shown that, for an Oldroyd-B fluid, the instability persists for $\beta \sim 0.2$, where β is the ratio of solvent to total solution viscosity.

IV. CONCLUSIONS

A linear stability analysis was carried out for plane Couette flow of a UCM fluid past a linear elastic solid in the low Reynolds number limit, using both asymptotic and numerical methods. We examined the effect of the nondimensional solid elasticity parameter Γ and the Weissenberg

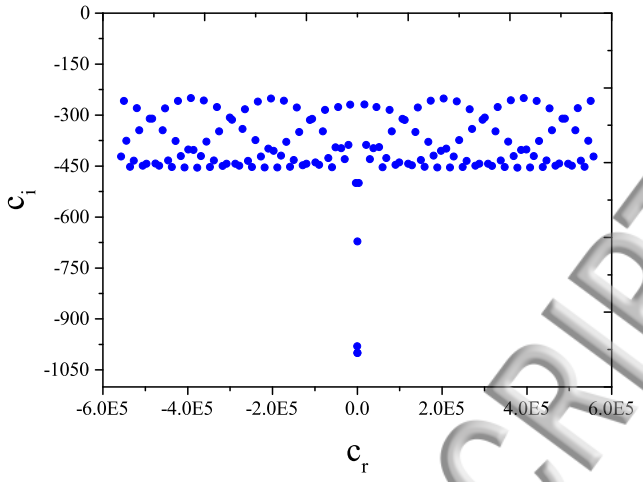

FIG. 13: Eigenspectrum for plane Couette flow past a deformbale wall at $Re = 10^{-4}$, $W = 10^{-3}$, $\Gamma = 10^{-4}$, $k = 1$, $H = 1$, at $\frac{W}{\Gamma} = 10$.

number W on the HFGL modes and the eigenmodes that represent shear waves in the elastic solid. An important result from the present study is the identification of resonance between shear waves in the viscoelastic fluid and elastic solid. For a fixed Re and Γ, a gradual increase in W leads to a condition where the HFGL and solid eigenspectra merge. The decay rates of HFGL modes decrease while the decay rates of shear waves in the solid increase, with an increase in W, a trend that continues until both the eigenspectra resonate. Resonance happens when the wave speed of solid eigenmodes $\sim \sqrt{\frac{G}{\rho}}$ is equal to the wave speed of HFGL modes $\sim \sqrt{\frac{\eta}{\tau_R \rho}}$, and the coupled flow system acts as a single continuum characterized by $c_i = \frac{-1}{2k(W+\Gamma)}$. We further showed that increase in fluid inertia destroys the resonance and the merged (resonant) eigenspectrum decouples to give two separate eigenspectra for HFGL and solid eigenmodes.

The deformable solid has a stabilizing effect when $H < 1$, but has a destabilizing effect on the coupled flow system for $H > 1$. However, it is important to note that H does not participate in the decoupling phenomenon, and merely has a small effect on the structure of the resonated eigenspectrum. It introduces wavy patterns close to $c_r = 0$, which may affect the qualitative nature of the eigenspectrum for very small or large values of H. We examined the effect of $\frac{W}{\Gamma}$ ratio on structure of the eigenspectrum, and when $\frac{W}{\Gamma} = 1$, both solid and HFGL eigenspectrum resonate and the coupled fluid-solid system behaves as a single continuum. When the ratio $\frac{W}{\Gamma}$ is 0.1 (or, in general, less than 1), the fluid and solid modes start merging and form complex structures in the resulting eigenspectrum. We find that even if the $\frac{W}{\Gamma} \geq 0.1$, there must be a minimum value of both W and Γ with the ratio of two being 0.1 or more, in order for the interaction of eigenspectra.

The previous study of Kumar and Shankar[22] performed asymptotic analysis only up to leading order for UCM plane Couette flow and concluded that the wave speed is purely real for a rigid channel. In the present work, we obtained the first correction to the wave speed and showed that the asymptotic results agree well with our numerical results for flow in rigid channels. In order to accurately predict the stability of the UCM plane Couette flow past a flexible surface, we also obtained the first correction to the wave speed. The results suggest that the growth rate obtained by asymptotic analysis up to first correction agree well with the spectral (numerical) results. To understand the origin of instability predicted by Kumar and Shankar[22], we performed

asymptotic analysis (only up to leading order) in the absence of flow for the coupled fluid-solid system. We found that the eigenmodes obtained at leading order for the no-flow analysis are purely real, whereas the eigenmodes obtained in the presence of flow results in a complex wave speed even at leading order. It can thus be concluded from the no-flow analysis that the instability predicted previously by Kumar and Shankar[22] is a flow-induced instability caused by resonant shear waves between the fluid and the elastic solid.

REFERENCES

[1]J. B. Grotberg and O. E. Jensen, "Biofluid mechanics in flexible tubes," Ann. Rev. Fluid Mech. **36**, 121–147 (2004).

[2]J. B. Grotberg, "Respiratory fluid mechanics," Physics of Fluids **23**, 021301 (2011).

[3]T. M. Squires and S. R. Quake, "Microfluidics: Fluid physics at the nanoliter scale," Rev. Mod. Phys. **77**, 977–1026 (2005).

[4]M. K. S. Verma and V. Kumaran, "A multifold reduction in the transition reynolds number, and ultra-fast mixing, in a micro-channel due to a dynamical instability induced by a soft wall," J. Fluid Mech. **727**, 407–455 (2013).

[5]A. Shrivastava, E. L. Cussler, , and S. Kumar, "Mass transfer enhancement due to a soft elastic boundary," Chem. Engg. Sci **63**, 4302–4305 (2008).

[6]V. Kumaran and P. Bandaru, "Ultra-fast microfluidic mixing by soft-wall turbulence," Chem. Engg. Sci **149**, 156–168 (2016).

[7]S. S. Srinivas and V. Kumaran, "Effect of viscoelasticity on the soft-wall transition and turbulence in a microchannel," J. Fluid Mech. **812**, 1076–1118 (2017).

[8]V. Shankar and V. Kumaran, "Stability of fluid flow in a flexible tube to non-axisymmetric disturbances," J. Fluid Mech. **408**, 291–314 (2000).

[9]V. Kumaran and R. Muralikrishnan, "Spontaneous growth of fluctuations in the viscous flow of a fluid past a soft interface," Phys. Rev. Lett. **84**, 3310–3313 (2000).

[10]V. Kumaran, G. H. Fredrickson, and P. Pincus, "Flow induced instability of the interface between a fluid and a gel at low Reynolds number," J. Phys. II France. **4**, 893–904 (1994).

[11]V. Gkanis and S. Kumar, "Instability of creeping couette flow past a neo-Hookean solid," Phys. Fluids **15**, 2864–2471 (2003).

[12]V. Gkanis and S. Kumar, "Stabilty of pressure-driven creeping flows in channels lined with a nonlinear elastic solid," J. Fluid Mech. **524**, 357–375 (2005).

[13]R. Patne and V. Shankar, "Absolute and convective instability in combined Couette-Poiseuille flow past a neo-Hookean solid," Phys. Fluids **29**, 124104 (2017).

[14]R. Muralikrishnan and V. Kumaran, "Experimental study of the instability of viscous flow past a flexible surface," Phys. Fluids **14**, 775–780 (2002).

[15]M. D. Eggert and S. Kumar, "Observations of instability, hysterisis, and oscillation in low-reynolds number flow past polymer gels," J. Colloid Interface Sci. **278**, 234–242 (2004).

[16]R. Neelamegam and V. Shankar, "Experimental study of the instability of laminar flow in a tube with deformable walls," Phys. Fluids **27**, 024102 (2015).

[17]V. Shankar, "Stability of fluid flow through deformable tubes and channels: An overview," Sadhana **40**, 925–943 (2015).

[18]V. Shankar and S. Kumar, "Instability of viscoelastic plane Couette flow past a deformable wall," J. Non-Newtonian Fluid Mech. **116**, 371–393 (2004).

[19]Gaurav and S. V., "Stability of pressure-driven flow in a deformable neo-Hookean channel," J. Fluid Mech. **659**, 318–350 (2010).

[20]V. A. Gorodtsov and A. I. Leonov, "On a linear instability of plane parallel Couette flow of viscoelastic fluid," J. Appl. Math. Mech. **31**, 310–319 (1967).
[21]M. Renardy and Y. Renardy, "Linear stability of plane Couette flow of an upper convected Maxwell fluid," J. Non-Newtonian Fluid Mech. **22**, 23–33 (1986).
[22]A. S. Kumar and V. Shankar, "Instability of high-frequency modes in viscoelastic plane couette flow past a deformable wall at low and finite reynolds number," J. Non-Newtonian Fluid Mech **125**, 121–141 (2005).
[23]P. Chokshi and V. Kumaran, "Stability of the flow of a viscoelastic fluid past a deformable surface in the low reynolds number limit," Phys. Fluids **19**, 104103 (2007).
[24]S. A. Roberts and S. Kumar, "Stability of creeping couette flow of a power-law fluid past a deformable solid," J. Non-Newtonian Fluid Mech. **139**, 93–102 (2006).
[25]M. Pourjafar, H. Hamedi, and K. Sadeghy, "Stability of power-law fluids in creeping plane poiseuille: Effect of wall compliance," J. Non-Newtonian Fluid Mech. **216**, 22–30 (2015).
[26]M. Pourjafar and K. Sadeghy, "Linear stability of shear-thinning fluids in deformable channels: Effect of inertial terms," J. Non-Newtonian Fluid Mech. **230**, 80–91 (2016).
[27]D. Giribabu and V. Shankar, "Stability of plane Couette flow of a power-law fluid past a neo-Hookean solid at arbitrary Reynolds number," Phys. Fluids **29**, 074106 (2017).
[28]V. S. Tanmay, R. Patne, and V. Shankar, "Stability of plane Couette flow of a carreau fluid past a neo-Hookean solid at arbitrary Reynolds numbers," Phys. Fluids **30**, 074103 (2018).
[29]M. K. S. Verma and V. Kumaran, "A dynamical instability due to fluid-wall coupling lowers the transition reynolds number in the flow through a flexible tube," J. Fluid Mech. **705**, 322–347 (2012).

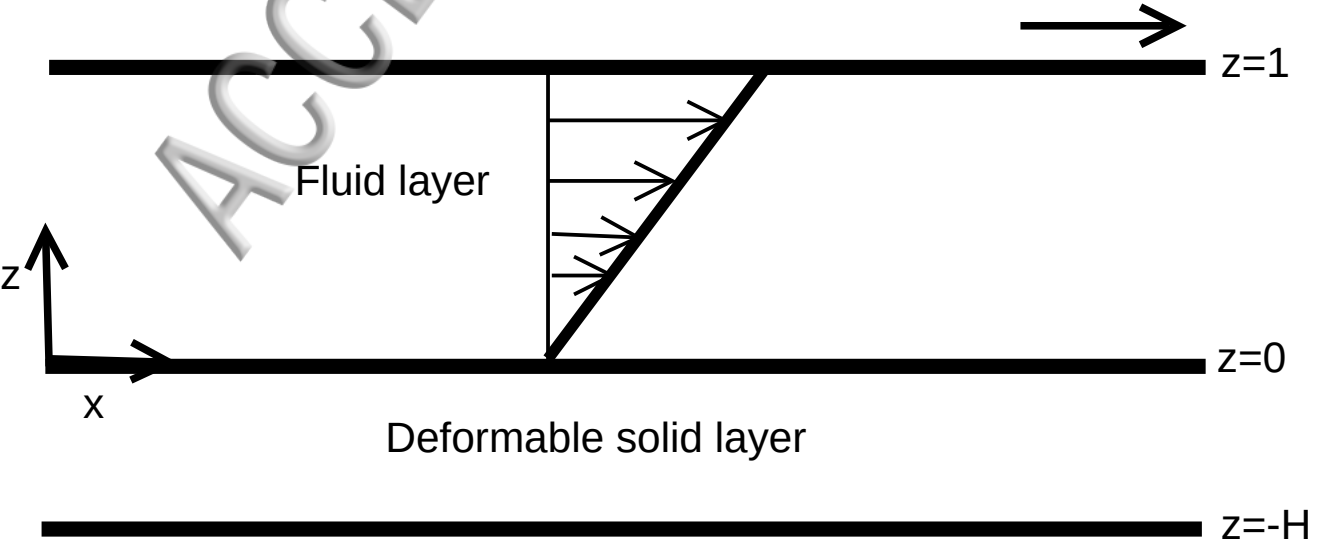
z=1
Fluid layer
z
z=0
x
Deformable solid layer
z=-H